International Journal of Climatology

RMetS Royal Meteorological Society

Global bimodal precipitation seasonality: A systematic overview

Journal:	*International Journal of Climatology*
Manuscript ID	JOC-17-0679.R3
Wiley - Manuscript type:	Short Communication
Date Submitted by the Author:	n/a
Complete List of Authors:	Knoben, Wouter; University of Bristol Department of Civil Engineering, Civil Engineering Woods, Ross; University of Bristol, Civil Engineering Freer, J; University of Bristol, School of Geographical Sciences
Keywords:	Climate < 2. Scale, Global < 2. Scale, Rainfall < 3. Physical phenomenon, Analytical framework, Bimodal seasonality
Country Keywords:	Kenya, Somalia, Sri Lanka, Indonesia, Colombia

Full title

Global bimodal precipitation seasonality: A systematic overview

Short title

Global bimodal precipitation seasonality: A systematic overview

Authors

1: Knoben, W.J.M.

2: Woods, R.A.

3: Freer, J.

Author affiliations

1: Department of Civil Engineering, University of Bristol, UK

2: Department of Civil Engineering, University of Bristol, UK

3: School of Geographical Sciences, University of Bristol, UK

Corresponding author

Knoben, W.J.M.

Woodland Road 93-95, Department of Civil Engineering, University of Bristol, BS8 1US, Bristol, UK

e: w.j.m.knoben@bristol.ac.uk

t/f: n/a

Sponsor

Engineering and Physical Sciences Research Council; EP/L016214/1

Abstract

Global precipitation patterns lead to differences in seasonal distributions of rainfall between locations, in the form of alternating dry and wet seasons. Many locations experience a single wet and dry season per year, but some studies report the occurrence of two wet and dry seasons per year. This bimodal rainfall pattern is commonly associated with locations within the tropics but is reported outside the tropics as well. However, this information is fragmented and studies of bimodality are mainly restricted to monthly rainfall totals. Here we use a gridded global data set and simple harmonic analysis to provide a systematic overview of global bimodal rainfall and rain-day frequency. We find a good agreement between the various regional studies concerning bimodal precipitation and our global overview, showing that bimodal rainfall occurs on approximately 7% of the global land surface. In the tropics, regions of bimodal rainfall totals (P) and regions of bimodal rain-day frequency (N) tend to overlap due to the presence of dry seasons that have zero precipitation. Outside the tropics P and N are more independent which leads to complex within-year patterns of precipitation intensity. A secondary outcome of our results is an improved low-dimensional global parameterisation of monthly rainfall regimes. Our results provide the first gridded global overview of bimodal rainfall patterns and show the usefulness of simple mathematical approaches for detecting patterns in large data sets.

Key words

Rainfall; bimodal seasonality; analytical framework; global climate

1 Introduction

Within-year climate patterns are a driving force behind environmental response in many locations. For example, the seasonal distribution of annual rainfall is important for large scale water resources planning and climate change impact assessment, because the seasonal availability of water influences society's need for reservoirs, flood defences, irrigation schemes, ecosystem management plans, etc. Seasonal precipitation patterns are complicated because they result from the interaction of large-scale climate factors with local topography (e.g. Soliman, 1953; Chang *et al.*, 2004; Poveda *et al.*, 2006; Herrmann and Mohr, 2011). Patterns vary from non-existent in arid regions, to having several alternating dry and wet seasons. We define this as a location's modality (unimodal being one wet and dry season per year; bimodal meaning two of each). This study investigates the global occurrence of bimodal precipitation (P) patterns and the accompanying number of rainfall events (N, days per month with $P \geq 0.1$mm, hereafter referred to as "rain-day frequency").

Early attempts to characterize rainfall seasonality rely on scattered station observations and include the use of a seasonality index in Africa, Australia and the US (Oliver, 1980) and harmonic analysis on a global scale (Hsu & Wallace, 1976). The seasonality index is unable to detect the differences between unimodal and bimodal regimes, but harmonic analysis can make this distinction. Later regional studies document bimodal precipitation patterns at a higher level of detail, here summarized by geographic region. The scattered nature of information makes it difficult to assess if, and unlikely that, this literature review covers all global occurrences of bimodal rainfall regimes. The tropics are relatively well-documented, although studies use different time periods, data sets, definitions and methods. Most observed rainfall patterns here are not bimodal, but either unimodal, constant or non-existent. Bimodal precipitation patterns outside the tropics seem similarly rare, although information on these

regions is even more fragmented. We did not locate any global study showing regions of bimodal rain-day frequency in the literature, though this too has occasionally been documented in local studies (e.g. Shahin, 2006; Malesu, 2006). Note that different authors assign different meanings to 'bimodal'. The term is either used to refer to alternating wetter and drier seasons or to the occurrence of two rainfall peaks within a single wet season. Additional ambiguity stems from the lack of consistency in the definition of 'wet' and 'dry' seasons. For example, the Pacific slope of the mountains of Panama experiences "a rainy season from late April-early May to late November, and a dry season in December-April, during which 2 [precipitation] maxima are witnessed in June and October" (Poveda *et al,* 2006). These precipitation peaks are reportedly 5 months apart but are considered to belong to a single rainfall season. The distinction between wet and dry seasons tends to be a relative assessment per location, depending on a study's purpose and method. In the short literature review in the following section, the term 'bimodal' is used to refer to alternating wetter and drier seasons (as reported in the cited publications). Two rainfall peaks within a single wet season are mentioned as such.

Bimodal precipitation in Latin and South America: Bimodal monthly precipitation patterns in Meso- and tropical South America are limited to the western Andean cordillera, central Colombia, the Venezuelan Andes, the Eastern Guyana Highlands (Poveda *et al.*, 2006) and certain Guyana coastal regions (Bovolo *et al.*, 2012). The remaining regions have chiefly unimodal precipitation patterns (Angeles *et al,* 2010; Poveda *et al.*, 2006; Nobre and Shukla, 1996). Precipitation over Mexico and Central America follows a dry winter, wet summer pattern. The summer season has a marked drop in precipitation during July and August known as the midsummer drought, but these months are still significantly wetter than the dry winter months (Magaña *et al.*, 1999; Westerberg *et al.*, 2010). This is also the case for Caribbean islands north of approximately 17°N (Angeles *et al,* 2010). Hsu & Wallace, (1980) also detect

some bimodal seasonality in central and north-eastern Argentina. **Africa:** Herrmann and Mohr (2011) investigate the African continent and find bimodal precipitation patterns in east Somalia, Ethiopia, Kenya and South-Sudan, confirmed by Owiti and Zhu (2012). Bimodal precipitation also occurs in coastal Côte d'Ivoire, Ghana and central Madagascar, along with dual peaks in a single wet season in adjacent regions (Herrmann and Mohr, 2011). One wet season with two peaks also occur scattered around the equator (Herrmann and Mohr, 2011). Soliman (1953) reports bimodal rainfall in southern Egypt. **Asia:** The tropical area of India is chiefly unimodal with a rainy season from July to September (Parthasarathy *et al.*, 1994), although the south-eastern regions receive their main rains from October to December (Chidambaram *et al.*, 2009). Western Sri Lanka has bimodal precipitation (Malmgren *et al.*, 2003). Chang *et al.* (2004) find mainly unimodal patterns in South-East Asia. Exceptions are the Malaysian peninsula, North-East Borneo and certain small islands on the equator. **Oceania:** Precipitation patterns in northern Australia are unimodal (Potter *et al.*, 2005). **Extratropics:** Examples of bimodal precipitation regimes outside the tropics include western Arizona in the USA (Hereford *et al.*, 2002), the Pyrenees region in southern Europe (Regüés and Gallart, 2004), central Egypt (Soliman, 1953) and the Indus delta in Pakistan (Rasul *et al.*, 2012). Sayemuzzaman and Jha (2014) report examples of major-minor wet seasons in coastal North Carolina. Keables (1989) reports two wet peaks during summer in the Upper Midwest USA, within a single wet season. Tang and Reiter (1984) further mention complex multi-modal (up to four annual peaks) rainfall patterns over the North American plateau, stretching from the Canadian Rocky Mountains south to the Mexican border. Herrmann and Mohr (2011) report bimodal rainfall in select regions in South Africa, Botswana, Namibia and Mozambique, in addition to scattered regions with two rainfall peaks in a single wet season. **Global:** the findings of Hsu & Wallace (1980) are generally confirmed by the regional studies cited above.

A variety of methods are used to determine whether bimodal rainfall occurs, including visual assessment of time series (e.g. Angeles *et al*, 2010), harmonic analysis (e.g. Chang *et al*, 2004; Owiti and Zhu, 2012) and rule-based data analysis (e.g. Herrmann and Mohr, 2011), depending on the size of the study area. For large study areas, simplified representations of global climate are often used to reduce data dimensionality. To this effect, harmonic analysis has been used to describe precipitation seasonality in the USA (Finkelstein and Truppi, 1991) and the tropics (Gershunov and Michaelsen, 1996; Chang *et al*, 2004; Owiti and Zhu, 2012). Several other studies use sinusoidal curves to describe monthly climate variables on a regional (e.g. Milly, 1994; Potter *et al.*, 2005) or global scale (Berghuijs and Woods, 2016). These studies calibrate a single harmonic with a 1-year period and assess how accurately this periodic function describes the original data. This approach has the advantage of compactly summarizing a climate variable's seasonality in three numbers with a clear physical interpretation: the mean value (corresponding to the monthly mean), the amplitude (describing the seasonality) and the phase (timing of the annual maximum). The studies that use sine curves apply these with a period of 12 months, giving a single peak per calendar year. Milly (1994), and Berghuijs and Woods (2016) suggested that a period of 6 months might be more appropriate for regions that experience bimodal rainfall patterns, but the effectiveness of this approach is so far unknown.

This paper builds on the framework presented in Berghuijs and Woods (2016) to create a systematic and objective overview of global bimodal precipitation (P) and rain-day frequency patterns (N), by comparing independent, truncated sinusoidal functions with 12-month and 6-month periods in their capability to reproduce observed monthly P and N. When a curve with a single peak is more accurate than a curve with two annual maxima, we define the local climate as unimodal (i.e. having one drier and one wetter season). Similarly, when the curve with two peaks is more accurate than the curve with a single peak, we define the local climate as bimodal. Using the relative accuracy of two simple mathematical descriptions to define

modality, we can avoid relying on subjective definitions of dry and wet seasons and avoid the use of empirical rules-based analysis.

2 Data

This study uses precipitation (P) and rain-day frequency (N) data directly obtained from the CRU TS v3.23 dataset (Harris *et al.*, 2014), which contains monthly climate values for both variables for the period 1901-2014 on the planet's land areas (except Antarctica). It is based on station observations combined with synthetic climatology and interpolated to a 0.5° latitude/longitude resolution. The study period is defined as 1984-2014, averaged into a typical year (e.g. the average January is based on the 30 monthly January values from years 1984-2014). This balances data quality (number of observations on which the gridded data is based declines sharply further away from the present, Harris *et al.*, 2014), the influence of interannual variability (due to using a relatively long period) and the influence of climate change (by using the most recent data).

We use four additional data sets of varying resolution to assess the robustness of our conclusions with respect to uncertainty in the climate data: Global Precipitation Climatology Centre (GPCC, 1984-2013, 0.5°x0.5° resolution, Schneider *et al.,* 2015), Global Precipitation Climatology Project (GPCP, 1984-2014, 2.5°x2.5° resolution, Adler *et al.,* 2003), Terrestrial Precipitation: 1900-2014 Gridded Monthly Time Series (TP, 1984-2014, 0.5°x0.5° resolution, Matsuura & Willmott, 2015) and Multi-Source Weighted-Ensemble Precipitation (MSWEP, 1984-2014, daily data aggregated to monthly scale, 0.25°x0.25° resolution, Beck *et al.,* 2017).

3 Methods

This study uses sinusoidal functions to approximate monthly averaged precipitation (P) and rain-day frequency (N) data of all global land cells on a 0.5° latitude/longitude resolution. Each

cell's P data is approximated with two independent sine curves, with a 12-month period (one annual peak) and 6-month period (two annual peaks) respectively. We quantify each curve's accuracy with an objective function defined as the average monthly error expressed as a percentage of the mean (Berghuijs and Woods, 2016). We assume that the sine curve with the lowest objective function value is the more appropriate description of the grid cell's climate, i.e. if the sine curve with period 6 months has a lower error than the 12-month period sine, we assume that the rainfall is bimodal. We apply the same procedure to the rain-day frequency data. A measure of the robustness of our conclusions follows from applying the sine-fitting method described above to 29 overlapping 3-year time windows in the 1984-2014 range and quantifying for how many periods each cell is classified as bimodal.

3.1 Sinusoidal functions

We use truncated sinusoidal functions that cannot reach physically unrealistic negative values to approximate monthly climate data (Berghuijs and Woods, 2016):

$$\hat{P}(t) = \max\left(0, \bar{P}\left[1 + C_r(\delta_P) + \delta_P \sin\left(2\pi \frac{t + 3 - s_P}{\tau}\right)\right]\right) \quad (1)$$

$$C_r(\delta_P) = -0.001 * \delta_P^4 + 0.026 * \delta_P^3 - 0.245 * \delta_P^2 + 0.2432 * \delta_P - 0.038 \quad (2)$$

$\hat{P}(t)$ is approximated monthly precipitation (mm), $\bar{P}$ the observed mean precipitation (mm), $C_r(\delta_P)$ an empirically derived correction factor which ensures that the mean of the truncated curve $\hat{P}(t)$ stays equal to $\bar{P}$, δ_P the fraction seasonal precipitation amplitude (-) and s_P the precipitation peak phase shift (months), which is shifted by an additional +3 months. The peak of a curve with $s_p = 0$ thus occurs in January, making non-zero s_p values easier to interpret. τ

is the curve's period [months]. The functions for rain-day frequency N (number of days per month with $P \geq 0.1mm$) are defined similarly:

$$\widehat{N}(t) = \max\left(0, \bar{N}\left[1 + C_r(\delta_N) + \delta_N \sin\left(2\pi \frac{t + 3 - s_N}{\tau}\right)\right]\right) \quad (3)$$

$$C_r(\delta_N) = -0.001 * \delta_N^4 + 0.026 * \delta_N^3 - 0.245 * \delta_N^2 + 0.2432 * \delta_N - 0.038 \quad (4)$$

These formulations necessarily mean that both peaks in the bimodal curve have the same amplitude. This limits the potential accuracy of our formulation to describe the data in locations where the climate is asymmetrical (e.g. when two annual dry seasons are of unequal length or severity). However, this limitation is required to keep the degrees of freedom the same between unimodal and bimodal formulations. Without this requirement, the accuracy metrics of both curves cannot be compared in a fair and meaningful way.

3.2 Calibration and evaluation

Parameters expressing the mean of the sine curve ($\bar{P}, \bar{N}$) are calculated directly as the mean of the data. Parameters δ (seasonal amplitude) and s (peak shift) are obtained through calibration by minimizing objective functions (eq. 5 and 6 respectively) using a multi-start Nelder-Mead simplex search method (Nelder and Mead, 1965; Lagarias *et al.*, 1998). The parameters are calibrated twice, once with seasonal length $\tau = 12$ [months] (from now called "unimodal sine") and once with $\tau = 6$ [months] ("bimodal sine").

This study concerns the typical seasonal pattern of climate variables. Therefore, the objective functions express the average error per month as a percentage of the mean (Berghuijs and Woods, 2016). This gives an overall impression of the sine curve's accuracy rather than focussing on a specific aspect such as getting the highest or lowest month captured accurately:

$$X_P = \frac{1}{12}\sum_{t=1}^{12}\frac{\left|\hat{P}(t) - P(t)\right|}{\bar{P}} \quad (5)$$

$$X_N = \frac{1}{12}\sum_{t=1}^{12}\frac{\left|\hat{N}(t) - N(t)\right|}{\bar{N}} \quad (6)$$

X_P shows the average simulated precipitation error (-) relative to the mean precipitation $\bar{P}$. $\hat{P}(t)$ are estimates of data $P(t)$ obtained using sine curves. The objective function for N is analogous to P.

We compare the accuracy of the calibrated unimodal and bimodal curves through simple subtraction (e.g. $\Delta X_P = X_{P,\tau=12} - X_{P,\tau=6}$) and interpret positive values to indicate the presence of a bimodal climate regime, because the bimodal curve better fits the data. These findings are compared to literature to judge the suitability of our method. We quantify our findings for both climate variables, assess the sensitivity of our conclusions to the choice of data period and comment on possible improvements to our scheme.

4 Results

Sine curves describing mean monthly precipitation totals (P, eq. 1) and rain-day frequency (N, eq. 3) are calibrated to fit observed monthly data using objective functions that minimise the average monthly error of each sine curve (eq. 5, 6 respectively). Using a seasonal duration τ = 12 (one peak per calendar year), the average global P error is 0.18 (-), median 0.15 (-), with standard deviation 0.10 (-) which is comparable to the findings in Berghuijs and Woods (2016). The average global N error is 0.12 (-), median 0.097 (-), with standard deviation 0.098 (-). In both cases larger errors occur mostly in locations with low annual precipitation (P < 240 mm/year, N < 30 days/year) or locations with hyperseasonal regimes (i.e. where the seasonal

range in P or N is larger than the mean). Changing the seasonal duration to $\tau = 6$ (two peaks per calendar year) results in improved accuracy of P approximations for 7.9% and 6.7% land cells in and outside the tropics respectively. Increased accuracy for N with $\tau = 6$ is obtained for 8.5% of tropical and 8.9% of extratropical cells respectively (Table 1).

Figure 1a (b) shows the best objective function value obtained for P (N), selecting the lowest option from unimodal and bimodal curves. Large errors occur mainly in drier areas where small absolute errors can be large relative to the mean. Figure 1c and 1d show the difference between unimodal and bimodal objective functions. A seasonal duration $\tau = 12$ is the more accurate option for most cells, but distinct areas with bimodal P and N are visible (areas with positive values, here bounded in red). Figure 1e and 1f shows how often each cell is classified as bimodal when the average climate of overlapping 3-year sub-periods is used, rather than the average climate of the full 1984-2014 period. Darker areas show more stable bimodality while light shading indicates that a bimodal sine outperforms the unimodal sine in only a fraction of the 29 sub periods. It is therefore likely that in the darker areas the seasonal pattern is indeed bimodal. In the lighter areas conclusions about the climate's modality are more sensitive to the choice of data period, possibly because the seasonal signal is occasionally obscured by interannual variability.

Bimodal rain and rain-day frequency areas tend to overlap in the tropics (5.9% of cells, Table 1). Alternating rain and no-rain seasons is a hypothesis that can explain this overlap in the tropics, because this would lead to similar within-year distributions of both variables (non-zero N values being conditional on non-zero P values). Outside the tropics zero-rain months are less common and bimodal regions overlap less (2.4% of cells), indicating that the within-year distributions of both variables can be very different. Furthermore, the appropriateness of either climate description changes gradually in space. For locations further away from the

equator, the difference between unimodal and bimodal sines is smaller than for locations close to the equator. Stronger climate seasonality in the tropics is a possible explanation, which can be investigated through the sine curve parameter values (Figure 2).

Figure 2e and 2f show the peak shift parameter in months away from January and are therefore represented on a circular colour scale. For areas with a seasonal length of 12 months, parameter values S_P and S_N of -6 and +6 months are equivalent. Within the red lines a seasonal length of 6 months is more accurate and here S_P and S_N values of -6, 0 and +6 months are equivalent. The parameter values do not give any explanation why the bimodal regions are where they are, because the seasonal pattern is governed solely by the chosen seasonal length (τ) of the fitted curves. However, the parameters do show that areas with larger objective function differences (Figure 1a, 1b) coincide with more extreme climates. These include arid and highly seasonal precipitation regimes in Africa (low $\bar{P}$, high δ_P), strongly seasonal P and N in India (high δ_P and δ_N values) and regions with a high number of rain events in Argentina (high $\bar{N}$ values). Peak timing parameters S_P and S_N are similar for most regions in the Southern Hemisphere, meaning P and N distributions are roughly in phase and thus the number of rainfall events goes up as monthly rainfall volumes increase. In the Northern Hemisphere P and N are more independent and the two distributions can be out of phase (e.g. Northern Europe). An increase in monthly rainfall totals thus does not necessarily lead to an increase in rainfall days, but might cause changes in the average rainfall per event.

5 Discussion

Previously, information about global bimodal precipitation was scattered across many different studies. This study uses gridded global climate data and simple mathematical analysis to create a systematic global overview of the location of bimodal precipitation regimes. To assess the sensitivity of our conclusions to data uncertainty, we have repeated the analysis

with four additional precipitation datasets. Across all data sets, the same regions are consistently identified as having bimodal rainfall climates (Figure 3). Figure 3c is a straightforward comparison of the CRU TS and GPCC data sets, showing that results are consistent for the majority of grid cells. The tropical locations generally align well with investigated literature, except for a region of Africa centred on the equator. Herrmann and Mohr (2011) classify this region as "humid" instead of bimodal. This definition of humid climates however depends on the minimum monthly rainfall in relation to the monthly temperature and not on the pattern of the monthly precipitation values, which has distinct wetter and drier (relative to the wet months) periods in this region. There are no other obvious instances within the tropics where our method indicates a bimodal rainfall regime but the available literature does not (deviations where our method indicates no bimodal regime but the literature does are discussed in a later section). Outside the tropics we see various cases where the bimodal sine curve is mathematically slightly more accurate than the unimodal sine (e.g. several locations in southern South America, large areas in the South-East USA, most of Greenland, certain Balkan areas and large regions of Southern Russia and Kazakhstan). However, the seasonal pattern in these areas is relatively asymmetrical and furthermore subject to strong interannual variations (as evidenced by Figure 1e, which shows that conclusions for these areas can change depending on the data period used). Combining the information about the accuracy of both curves with information about the sine curve parameters shows that in these regions the differences in accuracy between both curves are small ($|X_{P,\tau=12} - X_{P,\tau=6}| < 0.1$), but the accuracy of both is quite good ($X_P < 0.25$; compare figures 1a and 1c). From the parameter values we can deduce that these areas experience relatively high rainfall (figure 2a) and low seasonality (figure 2b). The seasonal pattern occurs on top of a high baseline rainfall, and the seasonal fluctuations in the pattern are thus relatively small compared to the overall signal. For certain locations regional studies report bimodal regimes

where one wet season has distinctly higher rainfall than the other wet season (i.e. Caribbean islands, Angeles *et al.*, 2010; Malaysian peninsula and several Indonesian islands, Chang *et al.*, 2004; scattered regions on the African continent, Herrmann and Mohr, 2011). Our method shows no clear improvement of bimodal sine curves over unimodal sines for these locations because our very simple bimodal sine curves are unable to replicate this specific behaviour. These regions show in our results as areas where the accuracy of both sine functions is similar (figure 1c, d) and low (figure1a, b), indicating that neither curve represents the seasonal pattern well (see also panels b and c in figure 5, where the asymmetry of the wet seasons causes the unimodal sine to be more accurate than the bimodal sine, although the objective function values show that both are inaccurate for this specific case). More complex mathematical formulations might have the required degrees of freedom to describe these regimes more accurately, but will necessarily have to sacrifice parsimony for improved accuracy. The 2-month long midsummer drought in Mexico and Central America , and similar patterns in other regions such as equatorial Africa, do not show up as bimodal in our results. In these cases, the stronger signal is the single wet season as described by the unimodal curve, and the double peaks within this single season are relatively minor fluctuations.

Figure 4 gives visual examples of the extent to which sine curves can capture the within-year variability, by comparing the accuracy of unimodal and bimodal curves for P and N at five different percentiles of $X_{\tau=12} - X_{\tau=6}$. The leftmost plots show that for certain locations the bimodal sine curve gives only a marginal improvement over the unimodal sine and that for other cases neither sine curve is a very appropriate description of the local climate. The actual errors between simulated and observed values are quite low for these specific instances and the climate might be considered constant instead of uni- or bimodal. The rightmost plots are in the top 2.5% of improvements and show that a bimodal sine curve can be good approximation of seasonal patterns. The unimodal sine is unsuitable for these cases, being either a straight

line (N) or completely missing the peak events in both magnitude and timing (P). The middle columns show examples where a bimodal sine is more appropriate than a unimodal sine, but unable to capture the within-year variability properly. These cases provide a visual example of bimodal sines correctly detecting a bimodal regime, but lacking mathematical freedom to simulate the seasonal pattern accurately.

However, even if this method is a rough approximation of local climates, comparing the accuracy of unimodal and bimodal curves gives insight into how climates change gradually in space on a global scale. We can interpret the difference in accuracy (Figure 1c, 1d) from negative to positive as a unimodal regime being more likely, to a bimodal regime being more likely. This implies that a gradual change occurs between two extremes, with regimes in the middle that are neither clearly unimodal nor bimodal and/or where both mathematical formulations are inadequate. Figure 5 shows a longitudinal cross section of eastern equatorial Africa, where the climate gradually changes from asymmetrical bimodal (39°lon; the dry seasons have different lengths and the rainfall peaks have different heights) to more symmetrical bimodal (40.5°lon) to nearly unimodal rainfall (42°lon). For the first case, limitations in the bimodal sine curve formulation (fixed amplitude, 6-month period) make it unable to outperform the unimodal sine curve in objective function terms, even though the bimodal sine curve gives a better general idea of the rainfall seasonality. As the observed pattern shifts to a more symmetrical bimodal regime (+40.5° to +41.5°lon) the bimodal sine clearly outperforms the unimodal sine. Further east the rainfall regime slowly shifts to being more unimodal (one of the peaks gradually becomes lower) and the unimodal sine becomes a more appropriate choice, as is reflected by its improved objective function value. Even though the asymmetry in bimodal regimes is not captured, this example shows that gradual changes in dominant climate patterns can be detected with this method.

This work provides insight in the sequence of dry and wet seasons on a global scale, and the relative importance of these intra-annual variations compared to the baseline signal. Strong intra-annual precipitation variability can be seen in much of the Southern Hemisphere (figure 1c), expressed as one of our mathematical formulations being much more accurate than the other. In these regions, the rain-day frequency pattern tends to be correlated with the precipitation (total) pattern, implying that the number of rain-days and precipitation total are conditional on one another. This is less so for much of the Northern Hemisphere, where the intra-annual precipitation variability is relatively small compared to the baseline (mean precipitation) and the rain-day frequency follows a more independent seasonal pattern. As a low-dimensional parametrisation of monthly rainfall regimes, these mathematical functions are an objective way to determine the strength of modality, they show spatial changes in climatic seasonality as a gradual change instead of a jump between categories and create the possibility to attach physical meaning to the functions' parameters. This make them a useful tool in any large-scale climate study. For example, these methods can be applied to investigate whether global rainfall regimes experience shifts from unimodal to bimodal, and whether this occurs as a result of natural variability or if trends can be found.

6 Conclusions

This study provides a systematic global overview of where bimodal precipitation (P) regimes occur, along with information on bimodal rain-day frequency (N), based on gridded climate data. Before, this information was scattered throughout various regional studies using different data, methods and definitions. This work aims to introduce a measure of objectivity by using simple sinusoidal functions to describe monthly rainfall and rain-day frequency data, using formulations that allow for either one or two peaks per year. Comparing the average monthly error obtained by both formulations indicates whether a unimodal or bimodal climate

regime is more likely for a given location. Globally, bimodal precipitation occurs in approximately 7.1% of grid cells, divided into 7.9% of tropical cells and 6.7% of non-tropical cells. These results mostly confirm findings from regional studies, except one case due to definitions used in the regional study and several cases where the annual climate pattern is asymmetrical in either peak height or the respective length of dry and wet season(s), which is more complex than our simple formulations can describe. Overall, the spatial transition between unimodal and bimodal climates is gradual (e.g. north- and southwards of equatorial Africa and in northern Guyana), and our simple approach can detect these patterns. Sensitivity analysis shows that for areas in the transition zones between unimodal and bimodal (e.g. in north-eastern Kenya and northern Borneo), natural variability over a few years can cause the climate to switch back and forth between unimodal and bimodal. Within the tropics, the modality of rain-day frequency N tends to overlap with the modality of P, due to the occurrence of alternating dry and wet seasons with zero or low rainfall during the dry period. Outside the tropics, modality of P and N is more independent, which leads to complex changes in precipitation intensity during the year.

7 Acknowledgements

This work was funded by the EPSRC WISE CDT, grant reference number EP/L016214/1. We gratefully acknowledge the providers of the CRU TS, GPCP, GPCC, TP and MSWEP data for making their work publicly available. We thank Wouter Berghuijs and 3 anonymous reviewers for their helpful comments on earlier versions of this manuscript.

8 References

Adler, R. F., Huffman, G. J., Chang, A., Ferraro, R., Xie, P.-P., Janowiak, J., … Nelkin, E. (2003). The Version-2 Global Precipitation Climatology Project (GPCP) Monthly

Precipitation Analysis (1979–Present). Journal of Hydrometeorology, 4(6), 1147–1167. http://doi.org/10.1175/1525-7541(2003)004<1147:TVGPCP>2.0.CO;2

Angeles, M. E., González, J. E., Ramírez-Beltrán, N. D., Tepley, C. A., & Comarazamy, D. E. (2010). Origins of the Caribbean Rainfall Bimodal Behavior. *Journal of Geophysical Research Atmospheres*, *115*(11), 1–17. http://doi.org/10.1029/2009JD012990

Beck, H. E., Dijk, A. I. J. M. Van, Levizzani, V., Schellekens, J., Miralles, D. G., Martens, B., & de Roo, A. (2017). MSWEP: 3-hourly 0.25◦ global gridded precipitation (1979–2015) by merging gauge, satellite, and reanalysis data. Hydrology and Earth System Sciences, 21, 589–615. http://doi.org/10.5194/hess-21-589-2017

Berghuijs, W. R., & Woods, R. A. (2016). A simple framework to quantitatively describe monthly precipitation and temperature climatology. *International Journal of Climatology*. http://doi.org/10.1002/joc.4544

Bovolo, C. I., Pereira, R., Parkin, G., Kilsby, C., & Wagner, T. (2012). Fine-scale regional climate patterns in the Guianas, tropical South America, based on observations and reanalysis data. *International Journal of Climatology*, *32*(11), 1665–1689. http://doi.org/10.1002/joc.2387

Chang, C. P., Wang, Z., McBride, J., & Liu, C. H. (2004). Annual cycle of Southeast Asia - Maritime continent rainfall and the asymmetric monsoon transition. *Journal of Climate*, *18*(2), 287–301. http://doi.org/10.1175/JCLI-3257.1

Chidambaram, S., Prasanna, M. V., Ramanathan, A. L., Vasu, K., Hameed, S., Warrier, U. K., Srinivasamoorthy, K., Manivannan, R., Tirumalesh, K., Anandhan, P. & Johnsonbabu, G. (2009). A study on the factors affecting the stable isotopic composition in precipitation of Tamil Nadu, India. Hydrological Processes, 23(12), 1792–1800. http://doi.org/10.1002/hyp.7300

Finkelstein, P. L., & Truppi, L. E. (1991). Spatial-Distribution of Precipitation Seasonality in the United-States. *Journal of Climate*, *4*(4), 373–385. http://doi.org/10.1175/1520-0442(1991)004<0373:sdopsi>2.0.co;2

Gershunov, A., & Michaelsen, J. (1996). Climatic-scale space-time variability of tropical precipitation. *Journal of Geophysical Research-Atmosphere*, *101*(D21), 26297–26307. http://doi.org/10.1029/96JD01382

Harris, I., Jones, P. D., Osborn, T. J., & Lister, D. H. (2014). Updated high-resolution grids of monthly climatic observations - the CRU TS3.10 Dataset. *International Journal of Climatology*, *34*(3), 623–642. http://doi.org/10.1002/joc.3711

Hereford, R., Webb, R. H., & Graham, S. (2002). Precipitation History of the Colorado Plateau Region. In *U.S. Geological Survey Fact Sheet 119-02* (pp. 1–4).

Herrmann, S. M., & Mohr, K. I. (2011). A continental-scale classification of rainfall seasonality regimes in Africa based on gridded precipitation and land surface temperature products. *Journal of Applied Meteorology and Climatology*, *50*(12), 2504–2513. http://doi.org/10.1175/JAMC-D-11-024.1

Hsu, C.-P. F., & Wallace, J. M. (1976). The global Distribution of the Annual and Semiannual Cycles in Precipitation. Monthly Weather Review, 104(9), 1093–1101.

Keables, M. J. (1989). A Synoptic Climatology of the Bimodal Precipitation Distribution in the Upper Midwest. Journal of Climate, 2(11), 1289–1294.

Lagarias, J. C., Reeds, J. A., Wright, M. H., & Wright, P. E. (1998). Convergence Properties of the Nelder--Mead Simplex Method in Low Dimensions. *SIAM Journal on Optimization*, *9*(1), 112–147. http://doi.org/10.1137/S1052623496303470

Magaña, V., Amador, J. A., & Medina, S. (1999). The midsummer drought over Mexico and Central America. *Journal of Climate*, *12*(6), 1577–1588. http://doi.org/10.1175/1520-0442(1999)012<1577:tmdoma>2.0.co;2

Malesu, M. M. (2006). Rainwater harvesting innovations in response to water scarcity: The late experience. *Technical Manual No. 5.* World Agroforestry Centre.

Malmgren, B. A., Hulugalla, R., Hayashi, Y., & Mikami, T. (2003). Precipitation trends in Sri Lanka since the 1870s and relationships to El Niño-southern oscillation. *International Journal of Climatology*, *23*(10), 1235–1252. http://doi.org/10.1002/joc.921

Matsuura, K., & Willmott, C. J. (2015). Terrestrial Precipitation: 1900-2014 Gridded Monthly Time Series (Version 4.01).

Milly, P. C. D. (1994). Climate, soil water storage, and the average annual water balance. *Water Resources Research*, *30*(7), 2143–2156.

Nelder, J. A., & Mead, R. (1965). A Simplex Method for Function Minimization. The Computer Journal, 7(4), 308–313. http://doi.org/10.1093/comjnl/7.4.308

Nobre, P., & Shukla, J. (1996). Variations of Sea Surface Temperature, Wind Stress, and Rainfall over the Tropical Atlantic and South America. *Journal of Climate*. http://doi.org/10.1175/1520-0442(1996)009<2464:VOSSTW>2.0.CO;2

Oliver, J. E. (1980). Monthly precipitation distribution: A comparative index. Professional Geographer, 32(3), 300–309. http://doi.org/10.1111/j.0033-0124.1980.00300.x

Owiti, Z., & Zhu, W. (2012). Spatial distribution of rainfall seasonality over East Africa. *Journal of Geography and Regional Planning*, *5*(15), 409–421. http://doi.org/10.5897/JGRP12.027

Parthasarathy, B., Munot, A. A., & Kothawale, D. R. (1994). All-India monthly and seasonal rainfall series: 1871-1993. *Theoretical and Applied Climatology*, *49*(4), 217–224. http://doi.org/10.1007/BF00867461

Potter, N. J., Zhang, L., Milly, P. C. D., McMahon, T. A., & Jakeman, A. J. (2005). Effects of rainfall seasonality and soil moisture capacity on mean annual water balance for Australian catchments. *Water Resources Research*, *41*(6), 1–11. http://doi.org/10.1029/2004WR003697

Poveda, G., Waylen, P. R., & Pulwarty, R. S. (2006). Annual and inter-annual variability of the present climate in northern South America and southern Mesoamerica.

Palaeogeography, Palaeoclimatology, Palaeoecology, *234*(1), 3–27. http://doi.org/10.1016/j.palaeo.2005.10.031

Rasul, G., Mahmood, a, Sadiq, a, & Khan, S. I. (2012). Vulnerability of the Indus Delta to Climate Change in Pakistan. *Pakistan Journal of Meteorology*, *8*(16), 89–107.

Regüés, D., & Gallart, F. (2004). Seasonal patterns of runoff and erosion responses to simulated rainfall in a badland area in Mediterranean mountain conditions (Vallcebre, Southeastern Pyrenees). *Earth Surface Processes and Landforms*, *29*(6), 755–767. http://doi.org/10.1002/esp.1067

Sayemuzzaman, M., & Jha, M. K. (2014). Seasonal and annual precipitation time series trend analysis in North Carolina, United States. Atmospheric Research, 137, 183–194. https://doi.org/10.1016/j.atmosres.2013.10.012

Schneider, U., Becker, A., Finger, P., Meyer-Christoffer, A., Rudolf, B., & Ziese, M. (2015). GPCC Full Data Reanalysis Version 7.0 at 0.5°: Monthly Land-Surface Precipitation from Rain-Gauges built on GTS-based and Historic Data. http://doi.org/10.5676/DWD_GPCC/FD_M_V7_050

Shahin, M. (2006). *Hydrology and Water Resources of Africa* (illustrated). Springer Science & Business Media.

Soliman, K. H. (1953). Rainfall over Egypt. *Quarterly Journal of the Royal Meteorological Society*, *79*(341), 389–397.

Tang, M., & Reiter, E. R. (1984). Plateau Monsoons of the Northern Hemisphere: A Comparison between North America and Tibet. Monthly Weather Review, 112, 617–637. http://doi.org/10.1175/1520-0493(1984)112<0617:PMOTNH>2.0.CO;2

Westerberg, I., Walther, A., Guerrero, J., Coello, Z., Halldin, S., Xu, C., … Lundin, L. (2010). Precipitation data in a mountainous catchment in Honduras: Quality assessment and spatiotemporal characteristics. *Theoretical and Applied Climatology*, *101*(3), 381–396. http://doi.org/10.1007/s00704-009-0222-x

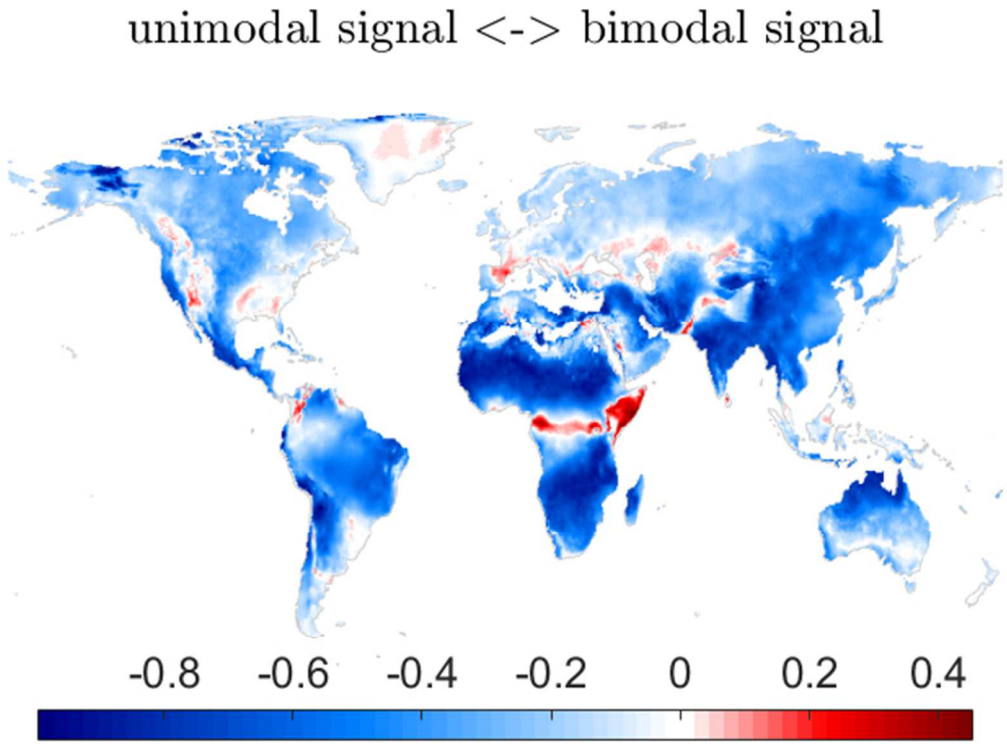

Global bimodal precipitation seasonality: A systematic overview

Knoben*, W.J.M., Woods, R.A., Freer, J.

This study uses gridded data and very simple mathematical analysis to create a first global overview of regions with bimodal precipitation seasonality. Approximately 7.1% of the global land surface is identified as having bimodal rainfall regimes. Sensitivity analysis shows that this seasonal pattern is relatively clear in the tropics, while outside the tropics interannual variability can obscure within-year seasonal patterns.

162x119mm (96 x 96 DPI)

		Global				Tropics				Non-tropics		
		P				P				P		
		$\tau = 12$	$\tau = 6$	Σ		$\tau = 12$	$\tau = 6$	Σ		$\tau = 12$	$\tau = 6$	Σ
N	$\tau = 12$	0.87	0.039	0.91		0.89	0.021	0.91		0.87	0.043	0.91
	$\tau = 6$	0.055	0.032	0.087		0.026	0.059	0.085		0.065	0.024	0.089
	Σ	0.93	0.071			0.92	0.079			0.94	0.067	

Table 1: Fraction of global grid cells where each combination of unimodal and bimodal P and N is most appropriate. Bimodal precipitation is slightly more common in the tropics than outside. Rain-day frequency shows no significant differences inside and outside the tropics.

995x182mm (96 x 96 DPI)

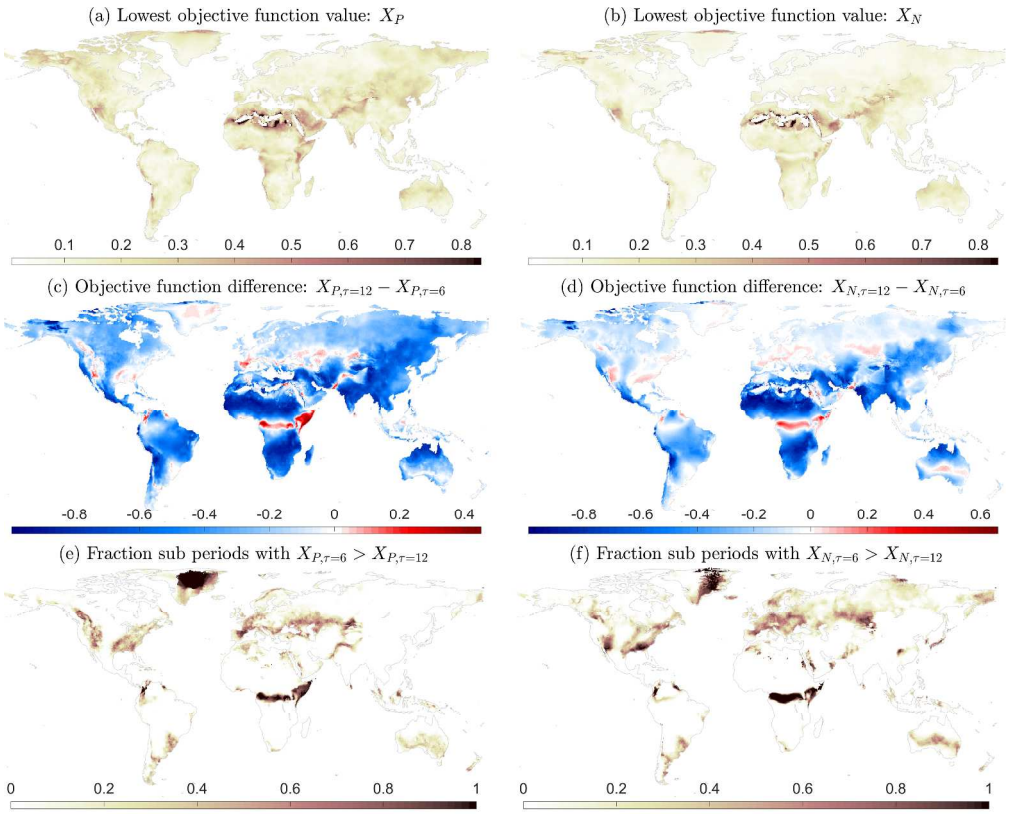

Figure 1: Calibration results from fitting sinusoidal functions to monthly averaged precipitation (P, left column) and rain-day frequency data (N, right column). Certain locations in the Sahara Desert show no objective function values as a mathematical artefact of there being no rainfall and no rain-days in the assessed period. (a, b) Lowest objective function value found for P and N respectively. (c, d) Difference between objective function values Xτ=12 and Xτ=6 for P and N respectively: lower (higher) values suggest that a seasonal length of 12 months (6 months) is more appropriate than the alternative. (e, f) Fraction of 3-year sub periods in the 1984-2014 data period in which a seasonal length of 6 months is more accurate than a seasonal length of 12 months.

472x381mm (300 x 300 DPI)

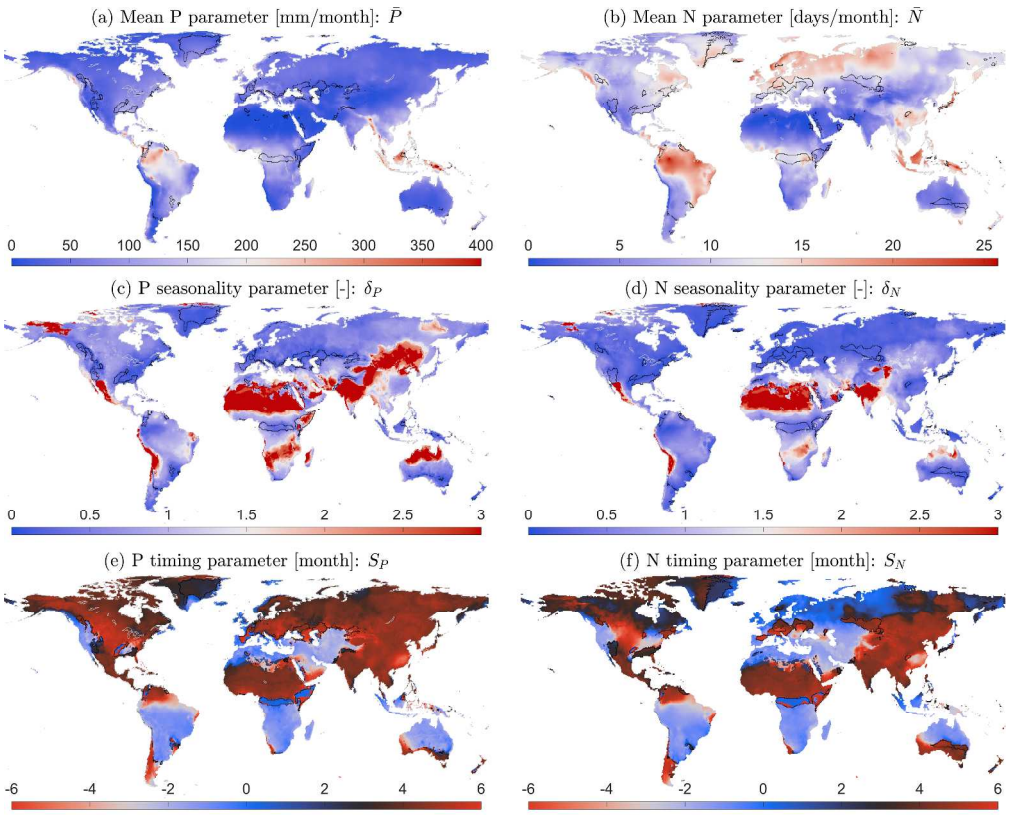

Figure 2: Parameter values for sine curves describing monthly average precipitation (P) and rain-day frequency (N), with areas where a seasonal length of 6 months is more appropriate than 12 months bounded in black. (a) Mean monthly P [mm], calculated from data; the scale is capped at 400mm to better highlight regional differences (0.06% of cells have values > 400mm/month). (c) P seasonality as a dimensionless multiplier of mean P; the scale is capped at 3 to better highlight regional differences (12.4% of cells have values > 3, predominantly in the extremely arid regions). (e) Timing of the P peak given in months away from January. (b) Mean monthly N [events/month], calculated from data. (d) N seasonality as a dimensionless multiplier of mean N, the scale is capped at 3 (5.8% of cells have values higher than 3, again predominantly in the very arid regions). (f) Timing of the N peak given in months away from January.

472x381mm (300 x 300 DPI)

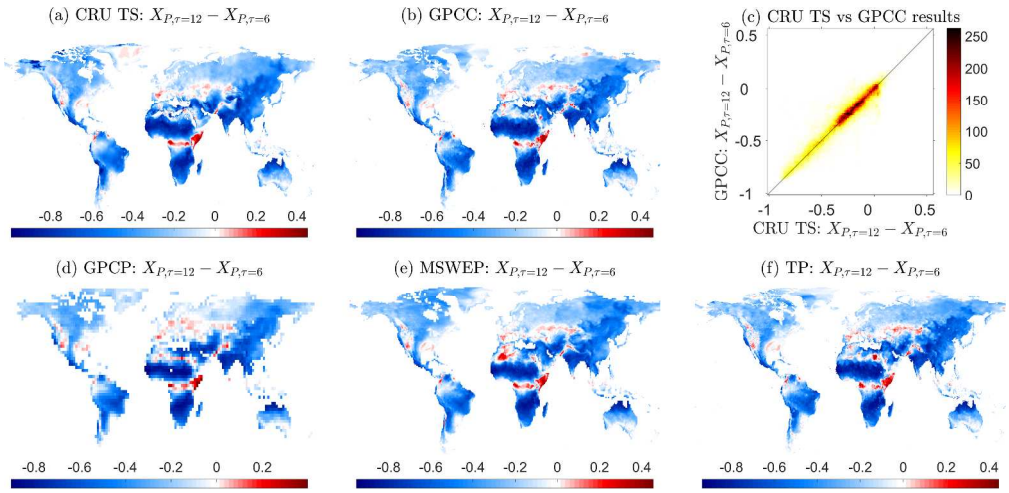

Figure 3: Stability of results under different precipitation data sets. Plot a, b, d, e and f show objective function differences between calibrated unimodal and bimodal sine curves for different data sets. (a) CRU TS data, 1984-2014, 0.5°x0.5° resolution, (b) GPCC data, 1984-2013, 0.5°x0.5° resolution, (c) overlap between CRU TS results and GPCC results, (d) GPCP data, 1984-2014, 2.5°x2.5° resolution, (e) MSWEP data, 1984-2014, 0.25°x0.25° resolution, (f) TP data, 1984-2014, 0.5°x0.5° resolution.

508x244mm (300 x 300 DPI)

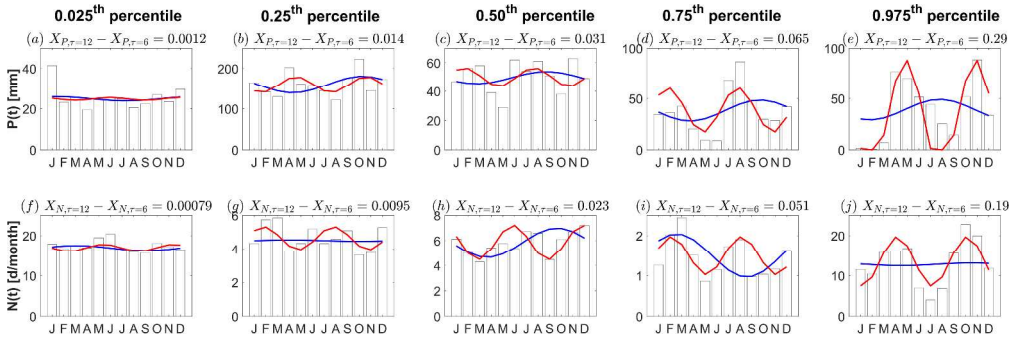

Figure 4: (a-e) 0.025th, 0.25th, 0.50th, 0.75th and 0.975th percentile respectively of locations where a bimodal sine curve is a better approximation of local rainfall regime than a unimodal curve is. (f-j) Similar plots for local rain-day frequency patterns. The leftmost plots indicate regions where both curves have similar accuracy; bimodal curves become more accurate compared to unimodal curves in the columns to the right.

503x165mm (300 x 300 DPI)

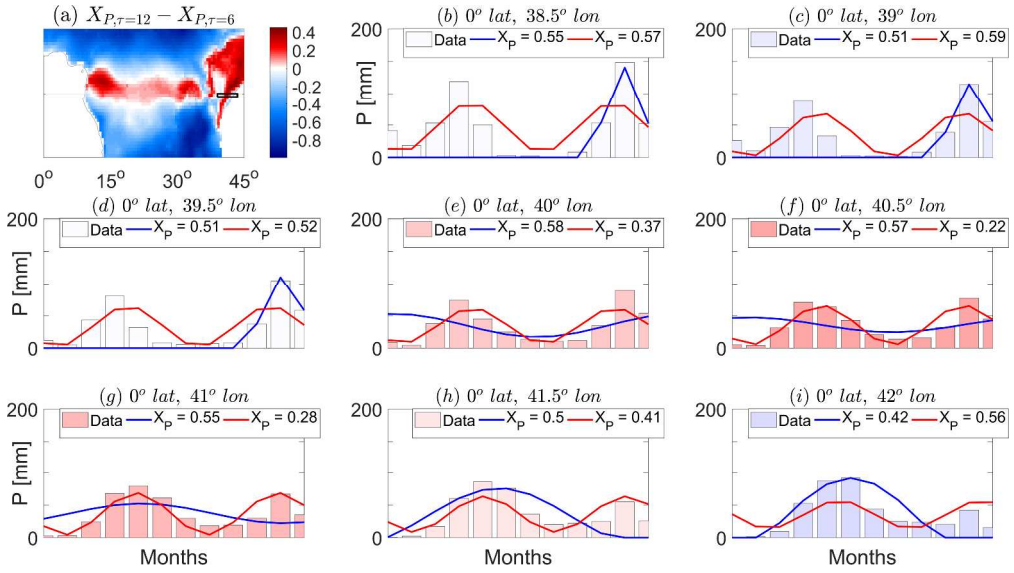

Figure 5: longitudinal cross-section of East Africa, showing average precipitation regimes. (a) Objective function difference between calibrated unimodal and bimodal sine curves. The red box indicates the locations where the following plots zoom in on. (b-i) Average precipitation regime (bars), calibrated unimodal sine curve (blue) and bimodal sine curve (red). Objective function (OF) values for both curves are given in the legend and data bars are coloured proportionally to which curve approximates the data more accurately. The images show a precipitation regime that gradually shifts from asymmetrical bimodal (a & b) to approximately symmetrical bimodal (f) to nearly unimodal (i).

411x230mm (300 x 300 DPI)